RSC Advances

ROYAL SOCIETY OF CHEMISTRY

www.rsc.org/advances

Cite this: DOI: 10.1039/c0xx00000x

www.rsc.org/xxxxxx

ARTICLE TYPE

Luminescence, energy-transfer and tunable color properties of a single-component Tb^{3+} or/and Sm^{3+} doped $NaGd(WO_4)_2$ phosphors with UV excitation for WLEDs

Yan Liu, Guixia Liu,* Xiangting Dong, Jinxian Wang and Wensheng Yu

Received (in XXX, XXX) Xth XXXXXXXXX 20XX, Accepted Xth XXXXXXXXX 20XX
DOI: 10.1039/b000000x

Tb^{3+} or/and Sm^{3+} co-doped $NaGd(WO_4)_2$ phosphors were prepared by a facile hydrothermal process, taking on flower-like microcrystals with a mean size of 3 μm. The $NaGd(WO_4)_2$: Sm^{3+} can efficiently absorb the ultraviolet light, and emit the bright blue light from the WO_4^{2-} group in the host, the yellow, orange and red emissions from the f-f transitions of Sm^{3+} by the host sensitization effect. Under the excitation of ultraviolet (405 nm), individual Sm^{3+} ions activated $NaGd(WO_4)_2$ phosphors generate excellent white and red light and the emission intensities reach the maximum at the Sm^{3+}concentration of 0.015, due to the concentration quenching effect occurring via a resonant type dipole-dipole interaction, of which the critical distance (R_{Sm-Sm}) is calculated to be 21.24 Å. More significantly, in the Tb^{3+} and Sm^{3+} co-doped $NaGd(WO_4)_2$ phosphors, the energy migration of Tb^{3+}-Sm^{3+} has been discussed to be dipole-dipole mechanism. In addition, under different ultraviolet radiation, the color-tunable emissions in $NaGd(WO_4)_2$: Tb^{3+}, Sm^{3+} microcrystals are realized, which could be favorable candidates in full-color phosphors for nUV-LEDs.

1 Introduction

Currently, white light-emitting diodes (WLEDs) have gained considerable attention as the hot spot in solid-state lighting areas owing to their attractive features such as excellent luminescent characteristics, good stability, high luminescence efficiency, as well as low cost[1-3]. At present, in view of conventional WLEDs with an unsatisfactory high correlated color temperature (CCT≈ 7750 K) and low color-rendering index (CRI≈ 70-80) for room lighting due to the color scarcity of the red emission, an near ultraviolet/ ultraviolet (n-UV/UV)-LED chip combined with tri-band, i.e., RGB (red, green and blue) phosphors have been suggested to achieve white light with high CRI and high power output [4-6]. Nevertheless the luminescence efficiency is inescapably impacted due to the reabsorption of blue light. Therefore, the fabrication of new full-color phosphors especially warm-white-emitting phosphors for WLEDs using a single component is one of the focus tasks challenging the solid state lighting technology. In order to generate multi-color emissions and upgrade the behaviour of white light with excellent quality, it is anticipated that efficient white emission could be realized by full-color emitting single-phase co-activated phosphors [7-12].

In consideration of the Sm^{3+} $^4G_{5/2}\rightarrow{}^6H_{J/2}$ (J= 5, 7, 9) characteristic emissions in the orange-red region respectively, Sm^{3+} ions are expected to possess superior red color purity [13-14]. However, Sm^{3+} ions have a weak absorption in UV region on account of the low oscillator strength. Due to this reason, on the basic of host-sensitizer sensitization effect, it is indispensable to choose a host that has intense and broad excitation bands in UV region utilized to sensitize Sm^{3+} ion emission. This phenomenon has been investigated in some inorganic hosts, such as molybdates[15], vanadates [16-17], phosphates [14] and borates [13], however, there is no report in $NaGd(WO_4)_2$ host as yet. The $NaGd(WO_4)_2$ host lattice belongs to the $CaWO_4$ family, which possesses fantastic features such as high UV absorption efficiency, self-activated characteristics. Hence, it is thought that the Sm^{3+}-doped $NaGd(WO_4)_2$ could be useful in a UV LED lighting system.

Moreover, as one of the most frequently used green emitters in rare earth ions doped materials, the Tb^{3+} mainly presents high efficiency characteristic emissions related to the large energy gap between the emitting state $^5D_{3,4}$ and the excited states ^7F_J (J= 2, 3, 4, 5, 6) for offering slight blue and intense green composition[18-19]. It is feasible to produce Tb^{3+} and Sm^{3+} co-activated warm-white-emitting phosphors by the combination of RGB emissions. Absorbingly, Tb^{3+} characteristic emissions from $^5D_3$ energy level overlap well with the $^6H_{5/2}\rightarrow{}^4D_{5/2}$, $^4K_{11/2}$, $^6P_{5/2}$, $^4G_{9/2}$ and $^4F_{5/2}$ transitions of Sm^{3+}. The Tb^{3+} sensitization effect has been utilized to sensitize Sm^{3+} ion emission in previous reports, where multicolor light were obtained used for WLEDs [14, 20] as well as some reports about Tb^{3+} and Sm^{3+} co-doping white phosphors in field emission displays [21-22]. In addition, it is noteworthy that extensive investigation of LED phosphors has been underway in recent years, in which co-doping a sensitizer and an activator into the same host is an efficient way to produce white-emitting by energy transfer between sensitizers and activators. Remarkably, the energy transfer process from Tb^{3+} to

Sm^{3+} has been investigated in some inorganic hosts, such as $Ca_2Gd_8Si_6O_{26}$ [21], $NaGdF_4$ [23], and $BaCeF_5$ [20].

Following this, in this work, we aim to focus our attentions on $NaGd(WO_4)_2$ as a host, Sm^{3+} and Tb^{3+} ions as activated ions. The color-tunable emissions in Sm^{3+} and Tb^{3+} co-doped $NaGd(WO_4)_2$ are realized by mainly combining Sm^{3+} orange red emissions with Tb^{3+} green light, besides the donation of limited blue emitting from WO_4^{2-} and Tb^{3+} $^5D_3$ characteristic transitions, and the sensitization effect of Tb^{3+}-Sm^{3+} ions. These phosphors are shown to be suitable for color-tunable and warm white phosphors for UV or near-UV WLEDs.

2 Experimental section

2.1 Materials

Aqueous solutions of $Gd(NO_3)_3$, $Tb(NO_3)_3$ and $Sm(NO_3)_3$ were obtained by dissolving the rare earth oxides Gd_2O_3, Tb_4O_7, Sm_2O_3 (99.99%) in dilute HNO_3 solution (15 mol/L) under heating with agitation in ambient atmosphere. All the other chemicals were of analytic grade and used as received without further purification.

2.2 Preparation

A series of rare earth-doped $NaGd(WO_4)_2$ phosphors were synthesized by a facile hydrothermal process without further sintering treatment. 1.0 mmol of $RE(NO_3)_3$ (including $Gd(NO_3)_3$, $Tb(NO_3)_3$ and $Sm(NO_3)_3$) were added into 100 mL flask. After vigorous stirring for 20 min, 2.0 mmol of $Na_2WO_4{\cdot}2H_2O$ was slowly added dropwise into the above solution. The pH was adjusted to 6-7. After additional agitation for 30 min, the resultant milky colloidal suspension was transferred to a 50 mL Teflon bottle held in a stainless steel autoclave, and then heated at 180 °C for 20 h. Finally, as the autoclave was naturally cooled to room-temperature, the precipitates were separated by centrifugation at 8000 r/min for 10 min, washed with deionized water and ethanol in sequence each several times, and then dried in air at 60 °C for 12 h.

2.3 Characterization

X-ray diffraction (XRD) was performed with a Rigaku D/max-RA X-ray diffractometer with Cu Kα radiation (λ= 0.15406 nm) and Ni filter, operating at a scanning speed of 10° min^{-1} in the 2θ range from 10 to 90°, 20 mA, 30 kV. The morphology and composition of the samples were observed by a FEI XL-30 field emission scanning electron microscope (FESEM) equipped with an energy-dispersive X-ray spectrometer (EDS). The excitation and emission spectra, and the luminescence decay curves of samples were measured using a HITACHI F-7000 Fluorescence Spectrophotometer equipped with a Xe lamp as the excitation source, scanning at 1200 nm/min. All of the measurements were performed at room temperature.

3 Results and discussion

3.1 Crystallization behavior and structure

The XRD patterns of $NaGd(WO_4)_2$ phosphors have been shown in Fig. 1. All the diffraction peaks of these samples can be exactly

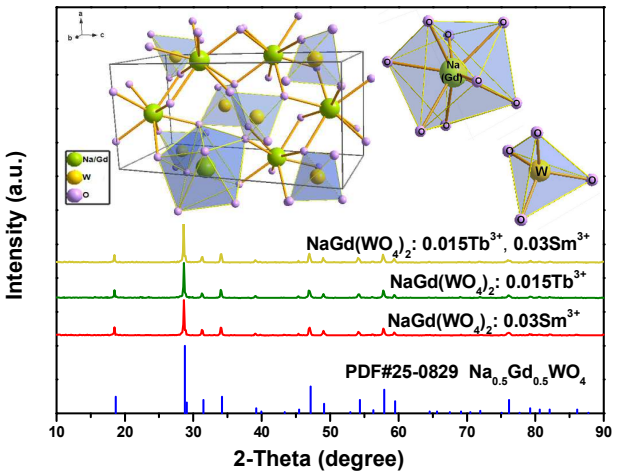

Fig. 1 XRD patterns of for $NaGd(WO_4)_2$: Tb^{3+}, Sm^{3+} phosphors; inset: the crystal structure of $NaGd(WO_4)_2$.

indexed to pure tetragonal phase of $NaGd(WO_4)_2$ and they match well with the standard values of PDF card (No. 25-0829) indicating that the doping ions do not impact significantly on the host structure. The $NaGd(WO_4)_2$ compound belongs to $CaWO_4$ type structure, which has the cell parameters of a = b = 5.243 Å, c = 11.368 Å and Z = 4. The crystal structure of $NaGd(WO_4)_2$ is shown in Fig. 1 (inset). When doping ions are introduced into the $NaGd(WO_4)_2$ host, in principle, it could prefer to occupy either of the two cation sites: eight-fold coordinated Na^+ (1.18 Å) sites and eight-fold coordinated Gd^{3+} (1.193 Å) sites. The effective radii of Tb^{3+} ions is 1.18 Å and Sm^{3+} ions is 1.22 Å for CN = 8. Comparison of ionic radii mismatch, both the two cation sites are probable host for doping ions (Tb^{3+} and Sm^{3+}), however, based on the valence state analysis, pointing that Gd^{3+} sites are much more probably to be occupied.

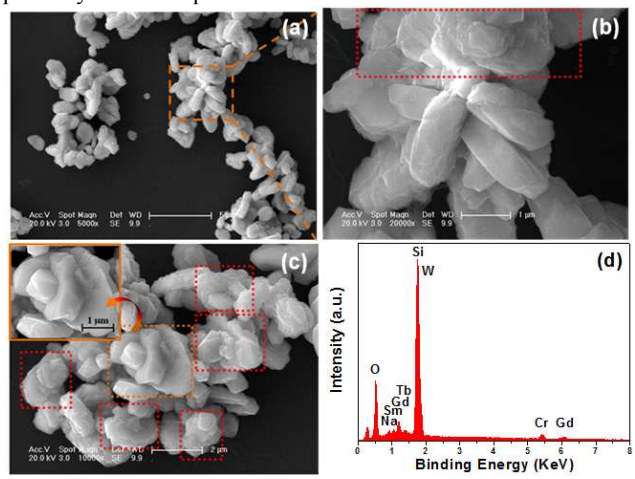

Fig. 2 FESEM images (a-c) and EDS pattern (d) of $NaGd(WO_4)_2$: Tb^{3+}, Sm^{3+} phosphor.

The morphology of $NaGd(WO_4)_2$: Tb^{3+}, Sm^{3+} is presented in Fig. 2a-c, and it takes on flower-like microcrystals with a mean size of 3 μm (shown in Fig. 2c) and few particles that have not grown completely. Fig. 2b is high magnification FESEM micrograph of selected area in Fig. 2a (dashed orange square). Clearly, it can be seen that these structures essentially generate via a layer-by-layer governing process. EDS pattern performs the

chemical composition of the product, containing Na, Gd, Tb, Sm, W, and O (silicon and chromium signals are from silicon host and spraying chromium process) (shown in Fig. 2d). Combined with above XRD patterns, the samples are further proved to be $NaGd(WO_4)_2$.

3.2 Photoluminescence properties of $NaGd(WO_4)_2$:Sm^{3+} phosphors

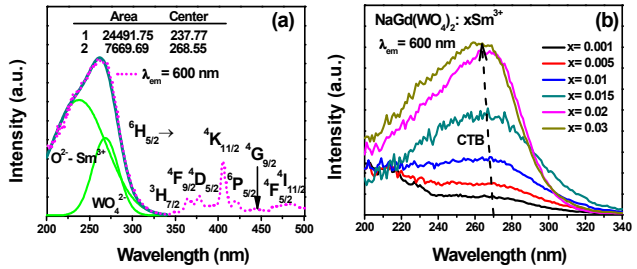

Fig. 3 PLE spectra for $NaGd(WO_4)_2$: $0.03Sm^{3+}$ phosphor (a) and PLE spectra for charge transfer from 200 to 340 nm of $NaGd(WO_4)_2$:xSm^{3+} (b).

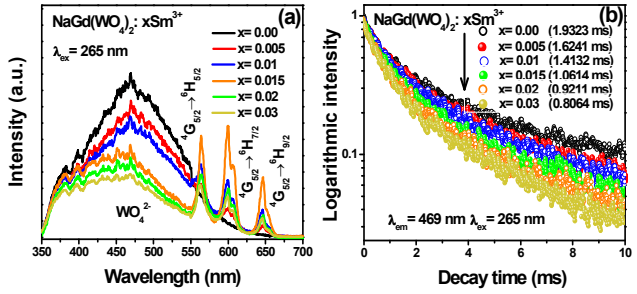

Fig. 4 PL spectra for $NaGd(WO_4)_2$:xSm^{3+} (λ_{ex}= 265 nm) (a); decay curves for the luminescence of WO_4^{2-} in $NaGd(WO_4)_2$:xSm^{3+} phosphors displayed on a logarithmic intensity (excited at 265 nm, monitored at 469 nm) (b).

Fig. 3a illustrates the photoluminescence excitation spectra for $NaGd(WO_4)_2$: $0.03Sm^{3+}$. As depicted in Fig. 3a, it can be seen that the PLE spectrum monitoring the orange emission of Sm^{3+} (600 nm, $^4G_{5/2}\rightarrow{}^6H_{7/2}$), consists of two components: the former is a strong and broad band from 200 to 340 nm with a maximum at 267 nm approximately which is attributed to charge transfer (CT) transitions of O^{2-}-Sm^{3+} from an oxygen 2p state excited to an Sm^{3+} 4f state and the O^{2-}-W^{6+} within the WO_4^{2-} groups, and the latter is the f-f transitions of Sm^{3+} in the longer wavelength region at 350, 365, 378, 405, 419, 444, 463, 483 nm corresponding to the electronic transitions of Sm^{3+} ions from the ground level $^6H_{5/2}$ to the $^3H_{7/2}$, $^4F_{9/2}$, $^4D_{5/2}$, $^4K_{11/2}$, $^6P_{5/2}$, $^4G_{9/2}$, $^4F_{5/2}$ and $^4I_{11/2}$ excited levels, respectively. It can be seen clearly that the strongest peak mainly exists at about 405 nm, indicating that the $NaGd(WO_4)_2$: Sm^{3+} phosphors are suitable to be used for near-UV LED excited phosphors. Furthermore, the CT transition from 200 nm to 400 nm can be deconvolved into two bands using Gaussian fitting shown in Fig. 3a. The peak located at 237 nm is due to the charge transfer band (CTB) between Sm^{3+} and O^{2-} whereas that centered at 268 nm is due to the CTB of WO_4^{2-} [8, 24]. The existence of O^{2-}-W^{6+} CT indicates energy transfer from WO_4^{2-} to Sm^{3+} in the $NaGd(WO_4)_2$: Sm^{3+} phosphors. This phenomenon illustrates that the excitation of the Sm^{3+} ions is partially through energy transfer from the WO_4^{2-} groups to the Sm^{3+} ions, but not all of the energy can be transferred to the Sm^{3+} ions so that upon excitation with 265 nm, $NaGd(WO_4)_2$: $0.02Sm^{3+}$ phosphor exhibits a board blue emission attributed to the transition of WO_4^{2-} in short wavelength region and three high intense emission peaks ascribed to the transitions of Sm^{3+} in long wavelength region (Fig. 4a). Therefore, tunable emission can be realized by combining the emission of the WO_4^{2-} groups and Sm^{3+} ions in a single host lattice under UV light excitation by different Sm^{3+} ions doping concentrations. Fig. 3b depicts the wavelengths of the charge transfer bands as a function of the Sm^{3+} concentrations in $NaGd(WO_4)_2$: xSm^{3+} phosphors. It is noted that by increasing the concentration of Sm^{3+}, the intensity of the CTB enhances, and the position of that shifts towards the higher energy region indicating the increase of the O^{2-}-W^{6+} CT energy. The CTB is related to the stability of the electron of the surrounding O^{2-} ions, i.e., the CT transition sensitive to the ligand environment (bonding energy between the central ion (M) and the ligand ions (L)) [4]. The CT energy, being directly proportional to M–L bond length, is inversely proportional to the M–L bond covalency. The substitution of Sm^{3+} ions with larger radius (1.22 Å) for Gd^{3+} ions (1.19 Å) generates the slight increase of W–O bond length, and then decreases the W–O bond covalency. Therefore, the CT energy increases.

To further understand the host-sensitizer sensitization effect, the luminescence intensities and the decay times of WO_4^{2-} in $NaGd(WO_4)_2$: xSm^{3+} phosphors with different Sm^{3+} concentrations are investigated. Fig. 4a depicts the PL spectra for $NaGd(WO_4)_2$: xSm^{3+} excited by charge transfer (CT) transition of O^{2-}-W^{6+} at 265 nm ($^1A_1\rightarrow{}^1B(^1T_2)$ transition). With the increase of Sm^{3+}, the emission intensities of Sm^{3+} gradually increase, but those of WO_4^{2-} in $NaGd(WO_4)_2$ host gradually decrease, which also supports that there is an energy transfer between Sm^{3+} and the WO_4^{2-}. The decay curves for the luminescence of WO_4^{2-} in $NaGd(WO_4)_2$:xSm^{3+} phosphors excited at 265 nm and monitored at 469 nm are measured and displayed in Fig. 4b. The corresponding luminescent decay curves can be fitted by a double-exponential equation

$$I = I_0 + A_1\exp(-t/\tau_1) + A_2\exp(-t/\tau_2) \quad (1)$$

And the average lifetime values are calculated using

$$\tau_{avg} = (A_1\tau_1^2 + A_2\tau_2^2) / (A_1\tau_1 + A_2\tau_2) \quad (2)$$

On the basis of equation (2), the average decay times for WO_4^{2-} are calculated and listed in Fig. 4b. The lifetimes for WO_4^{2-} are found to drastically decrease with increasing the Sm^{3+} concentration.

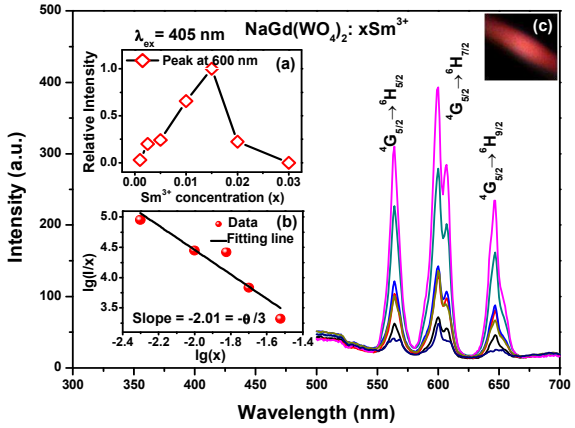

Fig. 5 PL spectra, dependence of relative emission intensity at 600 nm on Sm^{3+} concentration (inset, a), the relationship between Log(I/x) and Log(x) (inset, b) for $NaGd(WO_4)_2$:xSm^{3+} phosphors and the luminescence photograph of $NaGd(WO_4)_2$: $0.015Sm^{3+}$ (inset, c) (λ_{ex}= 405 nm).

The PL spectra of $NaGd(WO_4)_2$: xSm^{3+} phosphors are obtained by exciting at 405 nm (Fig. 5). Under 405 nm excitation, $NaGd(WO_4)_2$: xSm^{3+} phosphors give yellow, orange and red emissions, corresponding to the $^4G_{5/2}\rightarrow{}^6H_{5/2}$ (568 nm), $^4G_{5/2}\rightarrow{}^6H_{7/2}$ (600 nm) and $^4G_{5/2}\rightarrow{}^6H_{9/2}$ (648 nm) characteristic emissions of Sm^{3+} ions, respectively. The strongest one is located at 600 nm ($^4G_{5/2}\rightarrow{}^6H_{7/2}$). With increasing Sm^{3+} doping concentration due to the increase of luminescence centers, the dominating emissions enhance gradually first to an optimum concentration at 0.015, then decrease as a result of the concentration quenching, during which the excitation energy is lost to the killer sites non-radiatively [25] shown in Fig. 5 inset a. The concentration quenching of the Sm^{3+} emission is mainly due to the cross relaxation between neighboring Sm^{3+} ions which are in resonance of their energy levels: Sm^{3+} ($^4G_{5/2}$) + Sm^{3+}($^6H_{5/2}$) → Sm^{3+}($^6F_{9/2}$) + Sm^{3+} ($^6F_{9/2}$). The optimum concentration of Sm^{3+} is at a relatively low value in the $NaGd(WO_4)_2$ host lattice, which is attributed to the required approximately equal energy for the transitions of $^4G_{5/2}\rightarrow{}^6F_{9/2}$ and $^6H_{5/2}\rightarrow{}^6F_{9/2}$ of Sm^{3+} ions causing the concentration quenching of Sm^{3+} ions easy [24].

As an important parameter to evaluate the luminescence properties, the critical distance R_{Sm-Sm} between Sm^{3+} can be calculated using the concentration quenching method [26]

$$R_c = 2\times[3V/(4\pi x_c Z)]^{1/3} \quad (3)$$

where V is the volume of the unit cell, x is the concentration of Sm^{3+}, and Z is the number of available crystallographic sites occupied by the activator ions in the unit cell. For the $NaGd(WO_4)_2$ host lattice, V= 304.8 Å^3 and Z= 4. The critical concentration x_c, at which the luminescence intensity of Sm^{3+} is quenched, is 0.015. Therefore, the critical distance (R_{Sm-Sm}) of energy transfer is calculated to be about 21.24 Å. As the enhancement of Sm^{3+} concentration, the distance between Sm^{3+} ions becomes shorter than 21.24 Å, so the resonant energy transfer occurs between neighboring Sm^{3+} ions.

According to Van Uiter's report, it indicates that the interaction type between sensitizers or between sensitizer and activator can be calculated by the following [27-28]

$$I/x=k[1+\beta(x)^{m/3}]^{-1} \quad (4)$$

Where x is the activator concentration; I/x is the emission intensity (I) per activator concentration (x); k and β are constants; and when the value of m is 6, 8, or 10, the interaction corresponds to dipole−dipole (d−d), dipole-quadrupole (d−q), or quadrupole-quadrupole (q−q), respectively. From equation (4), it can be found that Log (I/x) acts as a linear function of Log(x) with a slope of -3/m. In order to well understand the energy transfer mechanism, we plotted the Log (I/x) versus Log(x) of Sm^{3+} in the $NaGd(WO_4)_2$: xSm^{3+} phosphors as shown in Fig. 5 inset b. The result of linear fitting presents that the slope is approximate to be -2.01 for $NaGd(WO_4)_2$: xSm^{3+} samples varying x from 0.01 to 0.03. Therefore, the calculated values of m is close to 6, meaning that the quenching results from dipole−dipole interactions in the $NaGd(WO_4)_2$: xSm^{3+} phosphors.

To further study the luminescence properties of Sm^{3+}, the fluorescence decay process of Sm^{3+} ions in $NaGd(WO_4)_2$: xSm^{3+} ($0.001\leq x\leq 0.02$) phosphors is investigated by monitored at 600 nm with irradiation of 405 nm. From Fig. 6, one can see that the decay behaviour of Sm^{3+} can be best fitted to the double-exponential model, employing equation (2), the lifetimes of Sm^{3+} ions are determined to be 1.6319, 1.0519, 0.8967, 0.8935 and 0.8613 ms, respectively. The lifetimes for Sm^{3+} ions are found to drastically decrease with increasing the Sm^{3+} concentration, which is ascribed to the increase of the nonradiative and self-absorption rate of the internal doped ions when activators cross the critical separation between donor and acceptor [29-30].

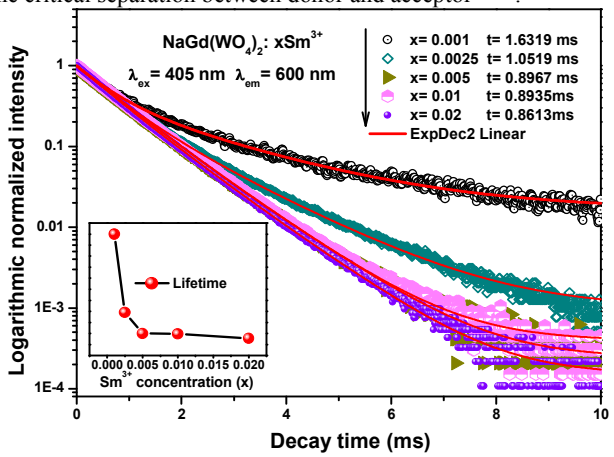

Fig. 6 Decay curves for the luminescence of Sm^{3+} ions displayed on a logarithmic intensity and inset: dependence of lifetimes on Sm^{3+} concentration in $NaGd(WO_4)_2$:xSm^{3+} phosphors (excited at 405 nm, monitored at 600 nm).

3.3 Photoluminescence properties of $NaGd(WO_4)_2$: Tb^{3+}, Sm^{3+} phosphors and energy transfer between Tb^{3+} and Sm^{3+} ions

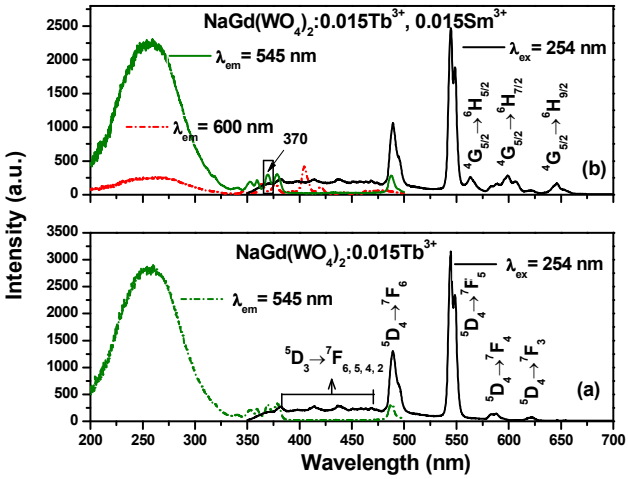

Fig. 7 PLE and PL spectra for $NaGd(WO_4)_2$:$0.015Tb^{3+}$ (a) and $NaGd(WO_4)_2$: $0.015Tb^{3+}$, $0.015Sm^{3+}$ (b) phosphors.

Fig. 7 shows the PLE and PL spectra for $NaGd(WO_4)_2$: $0.015Tb^{3+}$ (a) and $NaGd(WO_4)_2$: $0.015Tb^{3+}$, $0.015Sm^{3+}$ (b) phosphors. In Fig. 7a, it can be seen that the excitation spectrum of $NaGd(WO_4)_2$: $0.015Tb^{3+}$ (monitored at 545 nm) exhibits some absorption peaks at 340, 353, 359, 370, 378 and 487 nm assigned to the transitions of Tb^{3+} ions from the ground level $^7F_6$ to the $^5G_2$, $^5D_2$, $^5G_5$, $^5G_6$, $^5D_3$ and $^5D_4$ excited levels respectively, simultaneously includes a broad absorption band centred at 254 nm assigned to the CTB of WO_4^{2-} groups and f-d transition of Tb^{3+}. The f-f transitions of Tb^{3+} from 340 nm to 378 nm match well with the UV-LED chips indicating that $NaGd(WO_4)_2$: Tb^{3+} could be pumped by near-UV. Upon excitation at 254 nm, the $NaGd(WO_4)_2$: $0.015Tb^{3+}$ phosphor exhibits some weak blue emissions assigned to the $^5D_3\rightarrow{}^7F_{6,\,5,\,4,\,2}$ transitions (382, 414,

437, 469 nm), and two intense green emissions corresponding to the $^5D_4$-$^7F_6$ (490 nm) transition and dominant transition of $^5D_4$-$^7F_5$ (545 nm), besides slight yellow and red component ($^5D_4$-$^7F_4$ at 584 nm and $^5D_4$-$^7F_3$ at 624 nm), which could be a favourable candidate in green phosphors for nUV-LEDs. In Fig. 7b, when monitoring by the green emission of Tb^{3+} (545 nm) and orange emission of Sm^{3+} (600 nm), the PLE spectra of $NaGd(WO_4)_2$: $0.015Tb^{3+}$, $0.015Sm^{3+}$ illustrate some absorption peaks corresponding to the characteristic transitions of Tb^{3+} and Sm^{3+}, respectively. With 254 nm excitation, $NaGd(WO_4)_2$: $0.015Tb^{3+}$, $0.015Sm^{3+}$ phosphor yields the characteristic emissions of both Tb^{3+} and Sm^{3+} ions. Therefore, the tunable color could be generated by combining the green emissions of Tb^{3+} ions and orange-red emissions of Sm^{3+} ions via co-doping Tb^{3+} and Sm^{3+} ions in a single component.

To give direct evidence to demonstrate the Tb^{3+}-Sm^{3+} sensitization effect in the $NaGd(WO_4)_2$ host, it is needed to maximize the sensitization effect by fixing Tb^{3+} at high concentrations beyond quenching concentration. As shown in Fig. S1a-c, it can be clearly seen that the excitation spectra of Sm^{3+} ions in $NaGd(WO_4)_2$: $0.70Tb^{3+}$, $0.03Sm^{3+}$ and $NaGd(WO_4)_2$: $0.50Tb^{3+}$, $0.03Sm^{3+}$consist of typical Tb^{3+} and Sm^{3+} f–f excitation bands. Moreover, from Fig. S1d-f, the emission intensities of Sm^{3+} ions in $NaGd(WO_4)_2$: $0.70Tb^{3+}$, $0.03Sm^{3+}$ and $NaGd(WO_4)_2$: $0.50Tb^{3+}$, $0.03Sm^{3+}$ increase three times as that in $NaGd(WO_4)_2$: $0.015Tb^{3+}$, $0.03Sm^{3+}$ phosphor. In Fig. S2a, we choose 370 nm as excitation wavelength to pump $NaGd(WO_4)_2$: $0.015Tb^{3+}$ and $NaGd(WO_4)_2$: $0.015Tb^{3+}$, $0.15Sm^{3+}$ phosphors, respectively, because Tb^{3+} ions have absorption at 370 nm ($^7F_6 \rightarrow {}^5G_6$ transition), but Sm^{3+} ions have not. So In emission spectrum of Tb^{3+} excited at 370 nm, all the emission peaks belong to Tb^{3+} (dash line in Fig. S2a), but in $NaGd(WO_4)_2$: $0.015Tb^{3+}$, $0.15Sm^{3+}$ sample, (solid line in Fig. S2a) there are three peaks of Sm^{3+} at 568 nm ($^4G_{5/2} \rightarrow {}^6H_{5/2}$), 600 nm ($^4G_{5/2} \rightarrow {}^6H_{7/2}$) and 648 nm ($^4G_{5/2} \rightarrow {}^6H_{9/2}$) strongly attributed to the energy transfer from Tb^{3+} to Sm^{3+}. From Fig. S2b, we can distinctly see a significant spectra overlap between the emission of Tb^{3+} to Sm^{3+} in $NaGd(WO_4)_2$ host, which could further confirm the probability of energy transfer from Tb^{3+} to Sm^{3+}.

To further study the impact of doping concentration on the color-tunable emissions in a single component and energy migration process between activators, a series of phosphors with fixed Tb^{3+} ions concentration were prepared. Fig. 8a illustrates a series of emission spectra for $NaGd(WO_4)_2$: $0.015Tb^{3+}$, xSm^{3+} (x= 0.00, 0.005, 0.01, 0.02, 0.03, 0.05, 0.07, 0.09 and 0.15) under 254 excitation. Fixed the doping concentration of Tb^{3+} at 0.015, with increasing Sm^{3+} concentration, the emission intensities of the Sm^{3+} first increase to an optimum concentration at 0.03 then decrease due to the concentration quenching: Sm^{3+} ($^4G_{5/2}$) + Sm^{3+} ($^6H_{5/2}$) → Sm^{3+} ($^6F_{9/2}$) + Sm^{3+} ($^6F_{9/2}$) transitions, whereas that of the Tb^{3+} decreases monotonically, reflecting the result of energy transfer from Tb^{3+} to Sm^{3+}. Therefore, the luminescence intensities of various rare-earth ions can be enhanced or quenched by the energy transfer from other codoped rare-earth ions. The dependence of the emission color on the Sm^{3+} concentration in $NaGd(WO_4)_2$: Tb^{3+}, Sm^{3+} phosphors is shown in Fig.8b. With the increment of Sm^{3+} concentration, the $^4G_{5/2} \rightarrow {}^6H_{7/2}$ (Sm^{3+}) / $^5D_4$-$^7F_5$ (Tb^{3+}) ratio increase to be 0.5, those phosphors give abundant green, yellow, white and red emissions. Those illustrate the occurrence of energy transfer from Tb^{3+} to Sm^{3+} when they are codoped in the $NaGd(WO_4)_2$ host and provide a necessary condition for synthesizing the single phase full-color phosphors.

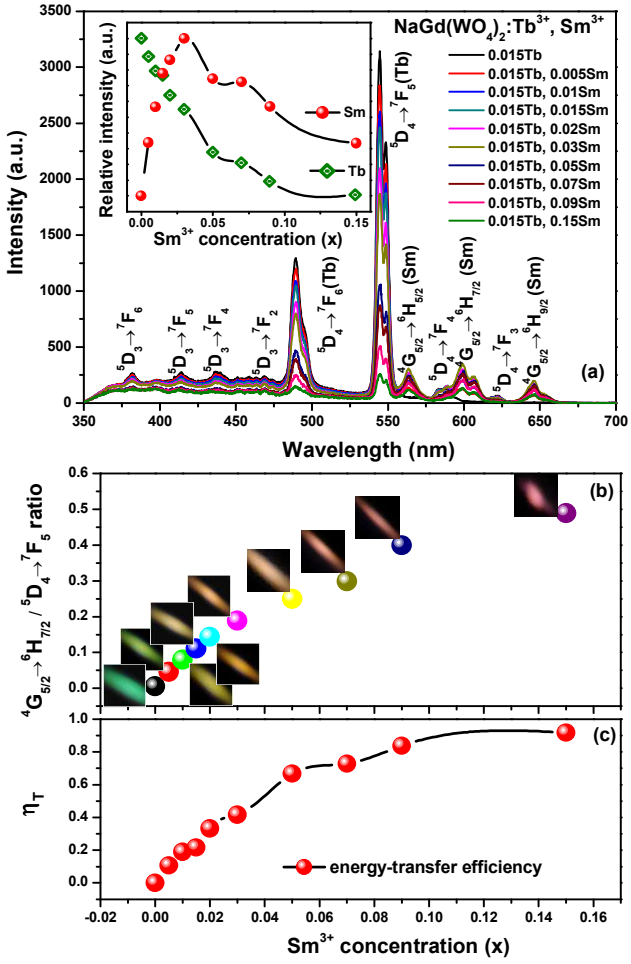

Fig. 8 PL spectra (excited at 254 nm) (a), the dependence of the emission color on the Sm^{3+} concentrations and corresponding luminescence photographs (b) and dependence of energy-transfer efficiency (η_T) on Sm^{3+} concentrations (x) (c) for $NaGd(WO_4)_2$:Tb^{3+}, Sm^{3+} phosphors.

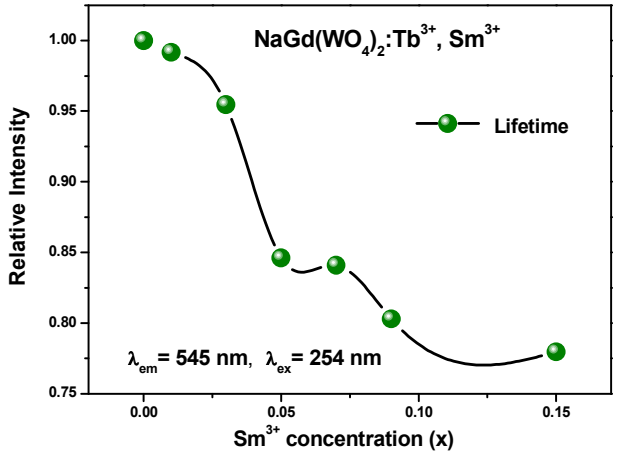

Fig. 9 Dependence of lifetimes on Sm^{3+} concentrations for $NaGd(WO_4)_2$:$0.015Tb^{3+}$, xSm^{3+} phosphors.

The energy-transfer efficiencies (η_T) from Tb^{3+} to Sm^{3+} are calculated using the following formula [30]

$$\eta_T = 1 - I/I_0 \quad (5)$$

where I and I_0 are the emission intensities for sensitizers with and without the acceptors ions. The energy transfer efficiency is calculated as a function of Sm^{3+} concentrations and is shown in Fig. 8c. The efficiency η_T increases gradually and reaches approximatively 92% at x=0.15. Moreover, the critical distance R_{Tb-Sm} of energy transfer from Tb^{3+} to Sm^{3+} can be calculated using equation (3), but here, the critical concentration x_c is defined as the total concentration of Tb^{3+} and Sm^{3+}, at which the luminescence intensity of Tb^{3+} is half of that in the absence of Sm^{3+}, is 0.055. Therefore, the critical distance (R_{Tb-Sm}) of energy transfer is calculated to be about 13.83 Å. As the enhancement of Sm^{3+} concentration, the distance between Tb^{3+} and Sm^{3+} becomes small enough (shorter than 13.83 Å), so the resonant energy transfer occurs: the energy difference between $^5D_4$ and $^7F_6$ of Tb^{3+} matches well with that between $^6H_{5/2}$ and $^4G_{7/2}$ of Sm^{3+}, which makes the energy migration from Tb^{3+} to Sm^{3+} efficient. The possible energy transfer mechanism is shown in Fig 12.

To further validate the process of energy migration, the fluorescence lifetimes for Tb^{3+} with different Sm^{3+} concentrations (x= 0.00, 0.01, 0.03, 0.05, 0.07, 0.09) are also measured and depicted in Fig. S3. As shown in Fig. S3a-e, the corresponding luminescence decay times can be best fitted to the double-exponential equation (1) determined to be 0.7586, 0.7524, 0.7241, 0.6418, 0.6380 and 0.6092 ms, respectively. The lifetimes of Tb^{3+} as a function of the Sm^{3+} concentrations in $NaGd(WO_4)_2$: $0.015Tb^{3+}$, xSm^{3+} phosphors is presented in Fig. 9. It can be clearly seen that the lifetimes for Tb^{3+} ions are found to drastically decrease with increasing the Sm^{3+} concentration.

In order to analyze the mechanism of energy-transfer process, we employ Dexter and Reisfeld's theory and Inokuti–Hirayama (I-H) model to deal with the luminescence intensity and fluorescent decay curves, respectively.

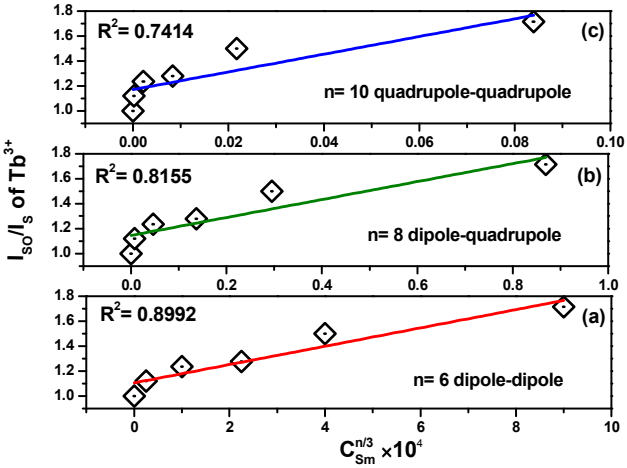

Fig. 10 The dependence I_{SO}/I_S of Tb^{3+} on the $C_{Sm}^{n/3} \times 10^4$ (n= 6, 8, 10) in $NaGd(WO_4)_2$:$0.015Tb^{3+}$, xSm^{3+} phosphors.

Based on Dexter's energy transfer formula of multipolar interaction and Reisfeld's approximation, the following equation can be used to analyze the potential mechanism [31-32]

$$I_{so}/I_s \propto C^{n/3} \quad (6)$$

where I_{so} is the intrinsic luminescence intensity of donors, and I_s is the luminescence intensity of donors in the presence of acceptors; and C is the doped concentration of acceptors. When the value of n is 6, 8, or 10, the interaction corresponds to dipole−dipole, dipole−quadrupole, or quadrupole−quadrupole, respectively. The I_{so}/I_s plots are illustrated in Fig. 10, and the plots are used linear fitting. It can be clearly seen that when n= 6, linear fitting result is the best, clearly implying the dipole–dipole interaction predominates in the energy transfer process between Tb^{3+} and Sm^{3+} ions.

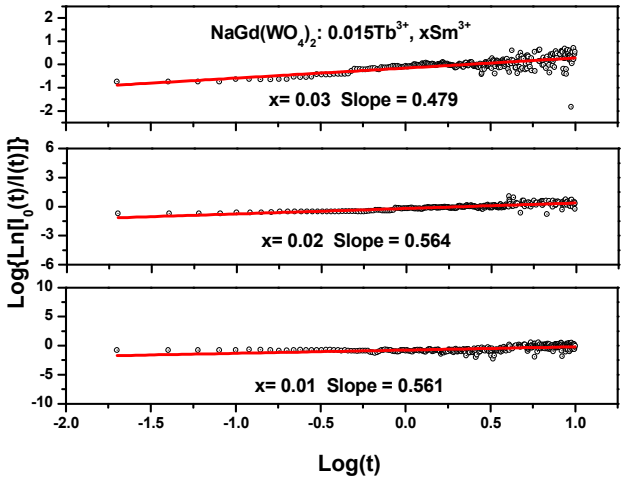

Fig. 11 Experiment data plots of Log{Ln[$I_0(t)/I(t)$]} versus Log(t) of Sm^{3+} in $NaGd(WO_4)_2$:$0.015Tb^{3+}$, xSm^{3+} phosphors.

According to the Inokuti–Hirayama (I-H) model to deal with the fluorescent decay curves, assuming that electric multipolar interaction, the modificatory decay function of excited donors due to energy transfer to the acceptors is given by the following equation [33]

$$I(t) = I_0(t) \exp[-4/3\pi\Gamma(1-3/S)n_A\alpha^{3/S}t^{3/S}] \quad (7)$$

where $I_0(t)$ characterizes the decay function of donors without the acceptors, n_A is the number of acceptor ions per unit volume, α is the rate constant for energy transfer, S= 6, 8, 10, the coefficient for dipole–dipole, dipole–quadrupole, and quadrupole–quadrupole interaction, respectively. From equation (7), it can be found that Log{Ln[$I_0(t)/I(t)$]} acts as a linear function of Log(t) with a slope of 3/S. We plotted the Log{Ln[$I_0(t)/I(t)$]} versus Log(t) of Sm^{3+} in the $NaGd(WO_4)_2$:$0.015Tb^{3+}$, xSm^{3+} phosphors as shown in Fig. 11. As the results of linear fitting shown, the slopes are approximate to be 0.561, 0.564 and 0.479 for $NaGd(WO_4)_2$:$0.015Tb^{3+}$, xSm^{3+} samples with x= 0.01, 0.02 and 0.03, respectively. Therefore, the calculated values of S are close to 6, indicating that the energy transfer from Tb^{3+} to Sm^{3+} occurs via the electric dipole–dipole mechanism, which is coincident with that analyzed above by Dexter and Reisfeld's theory.

A schematic model proposed for the probable ways of energy transfer in $NaGd(WO_4)_2$: Tb^{3+}, Sm^{3+} phosphors is shown in Fig. 12. During the excitation process, the electrons situated at oxygen 2p states absorb energies of photons from UV. As consequence of this phenomenon, the energetic electrons are promoted to tungsten 5d states located near the conductor band [34]. When the electrons fall back to lower energy states again via blue emission and energy transfer to Tb^{3+} and Sm^{3+} ions, and some energy is lost by cross relaxation.

The energy transfer among activator ions (Tb^{3+}, Sm^{3+}) offers

an approach to tune emission colors. Therefore, the CIE chromaticity coordinates for the phosphors excited at different wavelengths were determined based on their corresponding PL spectra, which are represented in the CIE diagram of Fig. 13 and the data is given in Tab. S1. $NaGd(WO_4)_2$: Sm^{3+} phosphor yields cool white emission under 270 nm radiation, whereas that gives pink light with excitation at 405 nm (Fig. 13, point a_1 and a_2). For the $NaGd(WO_4)_2$: Tb^{3+}, Sm^{3+} phosphors, the Tb^{3+} doping concentration is fixed at 0.015, as the concentration of Sm^{3+} increases from 0 to 0.15. It can be seen that when excited at 254 nm, the trend of their color tones changes from yellowish green to pink through warm white and the correlated color temperature becomes low gradually by adjusting the doping concentration of Sm^{3+}, the corresponding chromaticity coordinates and the correlated color temperature are presented in Fig. 13 (point b_3-j_3). Especially, there are five points at (0.400, 0.421), (0.412, 0.417), (0.432, 0.398), (0.433, 0.398) and (0.415, 0.348) with lower correlated color temperature of 3840, 3551, 3127, 2941, 2980 K, respectively, potentially find application in WLEDs. In addition, when excited by 365 nm those phosphors exhibit cool white emissions (point b_4, d_4, f_4, g_4 and h_4 in Fig. 13a) with higher correlated color temperature (> 8000 K) and the color changes to purplish pink (point i_4 in Fig. 13a) with a correlated color temperature at 5271 K, reflecting that the increasing of the Sm^{3+} concentration, the red component, could decrease the correlated color temperature at an exponential rate.

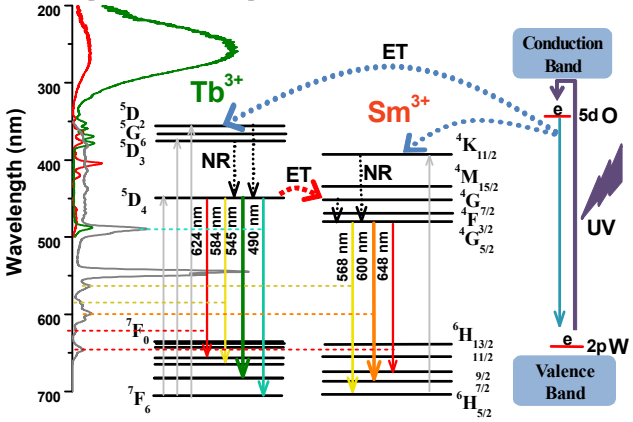

Fig. 12 Schematic energy-level diagram showing the excitation and emission mechanism of $NaGd(WO_4)_2$:Tb^{3+},Sm^{3+} phosphors (ET: energy transfer; NR: nonradiative).

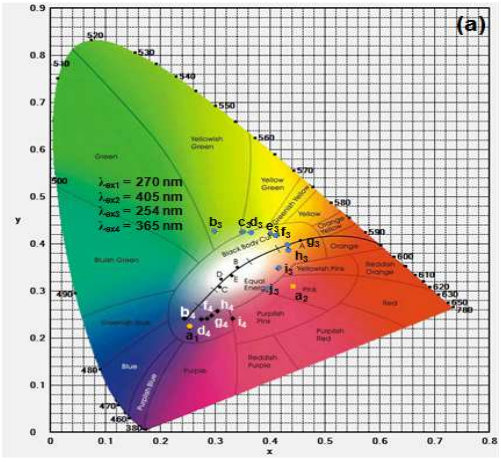

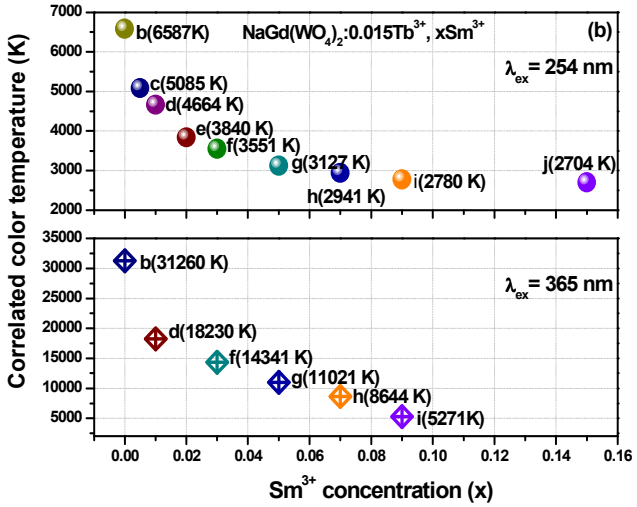

Fig. 13 CIE chromaticity diagram (a) and correlated color temperature (b) of the selected $NaGd(WO_4)_2$:Tb^{3+}, Sm^{3+} phosphors under different wavelengths excitation.

4 Conclusions

In summary, series novel color-tunable single-component $NaGd(WO_4)_2$: Tb^{3+}, Sm^{3+} phosphors were prepared by one-step hydrothermal method at 180 ℃ for 20 h. For $NaGd(WO_4)_2$: Sm^{3+} phosphors, Sm^{3+} ions generate intenser emission owing to the host-sensitizer sensitization effect. Under the excitation of ultraviolet, individual Sm^{3+} ions activated $NaGd(WO_4)_2$ phosphors exhibit excellent white and red emissions and the Sm^{3+} ions quenches at the concentration of 0.015 via a resonant type a dipole-dipole interaction. In the case of Tb^{3+} and Sm^{3+} co-doped systems, the efficient energy transfer process between Tb^{3+} →Sm^{3+} occurs via the dipole–dipole mechanism. Those single-component phosphors exhibit abundant color-tunable emissions besides warm white light with low correlated color temperature in the $NaGd(WO_4)_2$ host. Almost all of the prepared phosphors could find applications in WLEDs.

Acknowledgements

This work was supported by the National Natural Science Foundation of P.R. China (NSFC) (Grant No. **51072026**, **50972020**) and the Development of Science and Technology Plan Projects of Jilin Province (Grant No. **20130206002GX**).

Notes and references

Key Laboratory of Applied Chemistry and Nanotechnology at Universities of Jilin Province, Changchun University of Science and Technology, Changchun, China. Fax: +86-431-85383815; Tel: +86-431-85582574; E-mail: liuguixia22@163.com

1. T. Hashimoto, F. Wu, J. S. Speck and S. Nakamura, *Nat. Mater.*, 2007, **6**, 568-571.
2. T. Suehiro, N. Hirosaki and R. J. Xie, *ACS Appl. Mater. Interfaces,* 2011, **3**, 811-816.
3. S. Nakamura, T. Mukai and M. Senoh, *Appl. Phys. Lett.,* 1994, **64**, 1687-1689.
4. E. Pavitra, G. S. R. Raju, Y. H. Ko and J. S.Yu, *Phys Chem Chem Phys,* 2012, **14**, 11296-11307.

5. G. Seeta Rama Raju, E. Pavitra and J. S. Yu, *Dalton Trans.,* 2014, **43**, 9766-9776.
6. W. J. Yang and T. M. Chen, *Appl. Phys. Lett.,* 2007, **90**, 171908.
7. Y. Zhang, D. Geng, M. Shang, Y. Wu, X. Li, H. Lian, Z. Cheng and J. Lin, *Eur. J. Inorg. Chem.,* 2013, **2013**, 4389-4397.
8. X. Liu, W. Hou, X. Yang and J. Liang, *CrystEngComm,* 2014, **16**, 1268-1276.
9. N. S. Singh, N. K. Sahu and D. Bahadur, J. Mater. Chem. C, 2014, **2**, 548-555.
10. S. Unithrattil, K. H. Lee and W. B. Im, J. Am. Ceram. Soc., 2014, **97**, 874-879.
11. Z. W. Zhang, X. H. Shen, Y. S. Peng, Y. J. Ren and Z. Y. Mao, *Luminescence,* 2014.
12. W. Lu, Y. Jia, W. Lv, Q. Zhao and H. You, *New J. Chem.,* 2014, **38**, 2884-2889.
13. R. Satheesh Kumar, V. Ponnusamy and M. T. Jose, *Luminescence,* 2013, **29**, 649-656.
14. Y. Jia, W. Lu, N. Guo, W. Lu, Q. Zhao and H. You, *Chem. Commun.,* 2013, **49**, 2664-2666.
15. Y. Deng, S. Yi, Y. Wang and J. Xian, *Opt. Mater.,* 2014, **36**, 1378-1383.
16. W. L. Zhu, Y. Q. Ma, C. Zhai, K. Yang, X. Zhang, D. D. Wu, G. Li and G. H. Zheng, *Opt. Mater.,* 2011, **33**, 1162-1166.
17. V. Rao Bandi, B. K. Grandhe, M. Jayasimhadri, K. Jang, H. S. Lee, S. S. Yi and J. H. Jeong, *J. Cryst. Growth,* 2011, **326**, 120-123.
18. N. Yaiphaba, R. S. Ningthoujam, N. R. Singh and R. K. Vatsa, *Eur. J. Inorg. Chem.,* 2010, **2010**, 2682-2687.
19. Y. Zhang, D. Geng, M. Shang, X. Zhang, X. Li, Z. Cheng, H. Lian and J. Lin, *Dalton Trans.,* 2013, **42**, 4799-4808.
20. T. Sheng, Z. Fu, X. Wang, S. Zhou, S. Zhang and Z. Dai, *The J. Phys. Chem. C,* 2012, **116**, 19597-19603.
21. G. S. R. Raju, J. Y. Park, H. C. Jung, E. Pavitra, B. K. Moon, J. H. Jeong and J. H. Kim, *J. Mater. Chem.,* 2011**, 21**, 6136-6139.
22. G. Li, Z. Hou, C. Peng, W. Wang, Z. Cheng, C. Li, H. Lian and J. Lin, *Adv. Funct. Mater.,* 2010, **20**, 3446-3456.
23. H. Guan, G. Liu, J. Wang, X. Dong and W. Yu, *Dalton Trans.,* 2014, **43**, 10801-10808.
24. M. Shang, D. Geng, X. Kang, D. Yang, Y. Zhang and J. Lin, *Inorg. Chem.,* 2012, **51**, 11106-11116.
25. G. Blasse and B. C. Grabmaier, in *Luminescent Materials*, Springer Berlin Heidelberg, 1994, pp. 71.
26. G. Blasse, *Philips Res. Rep,* 1969, **24**, 131-144.
27. N. Guo, H. You, Y. Song, M. Yang, K. Liu, Y. Zheng, Y. Huang and H. Zhang, *J. Mater. Chem.,* 2010, **20**, 9061-9067.
28. L. G. Van Uitert, *J. Electrochem. Soc.,* 1967, **114**, 1048-1053.
29. Z. Xia, R. S. Liu, K. W. Huang and V. Drozd, *J. Mater. Chem.,* 2012, **22**, 15183-15189.
30. Z. Xia, Y. Zhang, M. S. Molokeev and V. V. Atuchin, *The J. Phys. Chem. C,* 2013, **117**, 20847-20854.
31. D. L. Dexter and J. H. Schulman, *J. Chem. Phys.,* 1954, **22**, 1063-1070.
32. R. Reisfeld, E. Greenberg, R. Velapoldi and B. Barnett, *J. Chem. Phys.,* 1972, **56**, 1698-1705.
33. H. Ohashi and N. Ii, *J. Japan. Assoc. Min. Petr. Econ. Geol.,* 1978, **73**, 267-272.
34. J. C. Sczancoski, L. S. Cavalcante, N. L. Marana, R. O. Silva, R. L. Tranquilin, M. R. Joya, P. S. Pizani, J. A. Varela, J. R. Sambrano, M. Siu Li, E. Longo, Andrés, J. *Curr. Appl. Phys.* 2010, **10**, 614-624.

Graphical Abstract

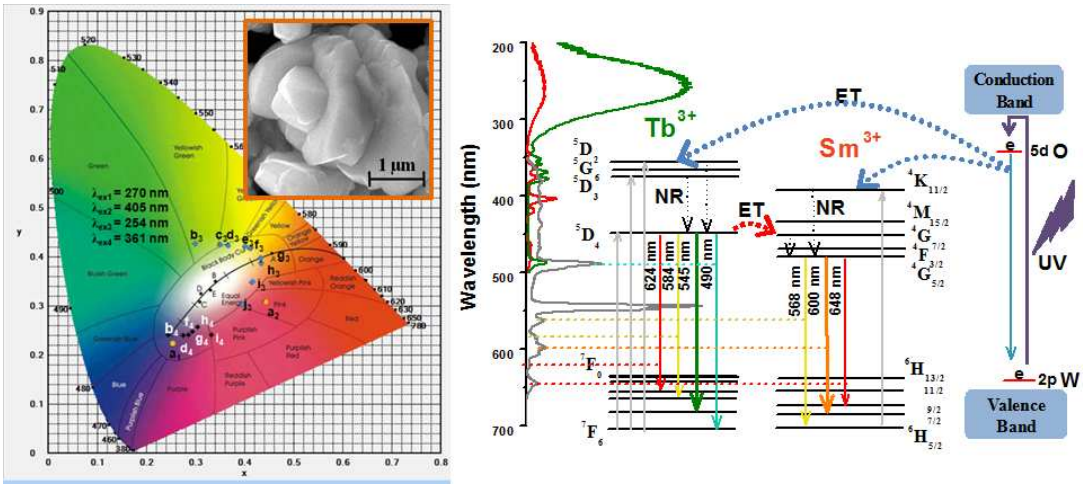

Tb^{3+} or/and Sm^{3+} co-doped $NaGd(WO_4)_2$ flower-like microcrystals were prepared by a facile hydrothermal process. Energy transfer mechanisms of WO_4^{2-}→ Sm^{3+} and Tb^{3+}→Sm^{3+} in the $NaGd(WO_4)_2$ host have been studied. Moreover, under different ultraviolet radiation, the color-tunable emissions in $NaGd(WO_4)_2$: Tb^{3+}, Sm^{3+} microcrystals are realized, which could be favorable candidates in full-color phosphors for nUV-LEDs.